

Three-Airy autofocusing beams

Xiao-Hong Zhang(张小红), Fei-Li Wang(王飞利), Lu-Yang Bai(白露阳), Ci-Bo Lou(楼慈波), Yi Liang(梁毅)

Citation: Chin. Phys. B . 2020, 29(6): 064204 . **doi:** 10.1088/1674-1056/ab84d2
Journal homepage: http://cpb.iphy.ac.cn; http://iopscience.iop.org/cpb

What follows is a list of articles you may be interested in

Far-field vector-diffraction of off-axis parabolic mirror under oblique incidence

Xia-Hui Zeng(曾夏辉), Xi-Yao Chen(陈曦曜)

Chin. Phys. B . 2020, 29(3): 034202 . **doi:** 10.1088/1674-1056/ab683e

A theoretical study of a plasmonic sensor comprising a gold nano-disk array on gold film with a SiO_2 spacer

Xiangxian Wang(王向贤), Jiankai Zhu(朱剑凯), Huan Tong(童欢), Xudong Yang(杨旭东), Xiaoxiong Wu(吴枭雄), Zhiyuan Pang(庞志远), Hua Yang(杨华), Yunping Qi(祁云平)

Chin. Phys. B . 2019, 28(4): 044201 . **doi:** 10.1088/1674-1056/28/4/044201

Propagation dynamics of off-axis noncanonical vortices in a collimated Gaussian beam

Cheng Yin(殷澄), Xuefen Kan(阚雪芬), Hailang Dai(戴海浪), Minglei Shan(单鸣雷), Qingbang Han(韩庆邦), Zhuangqi Cao(曹庄琪)

Chin. Phys. B . 2019, 28(3): 034205 . **doi:** 10.1088/1674-1056/28/3/034205

Propagation of a Pearcey beam in uniaxial crystals

Chuangjie Xu(许创杰), Ludong Lin(林露东), Zhengzhong Huang(黄郑重), Donglong He(何东龙), Dongmei Deng(邓冬梅)

Chin. Phys. B . 2019, 28(2): 024201 . **doi:** 10.1088/1674-1056/28/2/024201

Nonparaxial propagation properties of the chirped Airy Gaussian vortex beams in uniaxial crystals orthogonal to the optical axis

Yizuo Chen(陈奕佐), Guanwen Zhao(赵官文), Feng Ye(叶峰), Chuangjie Xu(许创杰), Dongmei Deng(邓冬梅)

Chin. Phys. B . 2018, 27(10): 104201 . **doi:** 10.1088/1674-1056/27/10/104201

Three-Airy autofocusing beams*

Xiao-Hong Zhang(张小红)[1], Fei-Li Wang(王飞利)[1], Lu-Yang Bai(白露阳)[1], Ci-Bo Lou(楼慈波)[1,†], and Yi Liang(梁毅)[2,‡]

[1] *Institute of Photonics, School of Physics Science and Technology, Ningbo University, Ningbo* 315211, *China*
[2] *Guangxi Key Laboratory for Relativistic Astrophysics, Center on Nanoenergy Research, School of Physics Science and Technology, Guangxi University, Nanning* 530004, *China*

(Received 16 January 2020; revised manuscript received 6 March 2020; accepted manuscript online 31 March 2020)

We numerically and experimentally demonstrate that a three-Airy autofocusing beam can be generated by superposing three deformed two-dimensional (2D) Airy beams with a triangle symmetry. When the initial angle between two wings of the deformed 2D Airy beams increases, such a three-Airy autofocusing beam exhibits that the focusing length decreases and the intensity contrast at the focal point changes. Moreover, after introducing an optical vortex phase, this three-Airy autofocusing beam displays a transverse rotation in propagation. The rotation angle is determined by the topological charge of the vortex and the initial wing angle. Our results may have some potential applications in optical manipulation.

Keywords: three-Airy autofocusing beam, triangle symmetry, optical vortex

PACS: 42.25.–p, 42.25.Fx, 42.30.Kq **DOI:** 10.1088/1674-1056/ab84d2

1. Introduction

Accelerating optical beams, represented by Airy beams, have attracted a lot of attention due to their unique properties including self-acceleration, self-reconstruction, and non-diffraction.[1–3] They have been used in various areas including optical micromanipulation,[4,5] filamentation,[6] light bullets,[7] optical routing,[8] imaging,[9–13] guiding discharges,[14] and material processing.[15] Triggered by the prosperity in optics, accelerating wave-packets were continuously realized in other wave systems such as plasmons,[16–18] acoustic waves,[19] electronic beams.[20]

In these different classes of applications, a special family of accelerating beams, namely, abruptly autofocusing (AAF) beams, plays an important role because of their autofocusing property.[21–27] The peak intensity for each of these beams almost is maintained at a constant level during early propagation, yet at a particular distance it abruptly increases by several orders of magnitude.[23–27] In general, the AAF beams are produced from radially symmetric Airy beams. In order to better control the autofocusing properties, many other methods were developed.[22–27] One can synthesize the AAF via a superposition of multiple one-dimensional (1D) or two-dimensional (2D) Airy beams distributed around a circle. Their autofocusing propagation is thus readily changed by engineering the lateral accelerations of the combining Airy beams. In these approaches, standard 2D Airy beams, for each of which the tangle between their two wings is the same, are employed. Recently, it was shown that the acceleration of 2D Airy beam changes with the angle between their two wings,[29–31] thus offering us an additional degree of freedom to control the AAF. Here, we propose a new kind of AAF beam via superposing three deformed 2D Airy beams with a triangle symmetry. Propagation dynamics of this new kind of AAF beam, namely, three-Airy autofocusing beam is investigated theoretically and experimentally. It is found that the three-Airy autofocusing beam definitely shows a focusing propagation and its focusing length varies with the angle between two wings of the superposing 2D Airy beam. Moreover, by engineering the phase profile of three-Airy autofocusing beam via a vortex structure, we can make the beams have a rotation. This rotation can be controlled by varying the topological charge of vortex structure and the initial wing angle. Our results will be very valuable for the optical manipulation.

2. Theoretical and experimental method

In the paraxial condition, the intensity distribution of a three-Airy autofocusing beam at different propagation positions can be defined as a sum of three 2D Airy beams

$$I(x,y,z) = \sum_m I_m(x,y,z),$$
$$I_m(x,y,z) = \frac{\exp(\mathrm{i}kz)}{\mathrm{i}\lambda z}\iint_{R^2}\varphi_m(x,y) \times \exp\left[\mathrm{i}k\frac{(x-x')^2+(y-y')^2}{2z}\right]\mathrm{d}x'\mathrm{d}y',$$

*Project supported by the National Natural Science Foundation of China (Grant No. 11604058), the Natural Science Foundation of Ningbo City, China (Grant No. ZX2015000617), the K C Wong Magna Fund in Ningbo University, China, and the Natural Science Foundation of Guangxi Zhuang Autonomous Region, China (Grant Nos. 2016GXNSFBA380244 and 2015GXNSFBA139011).

†Corresponding author. E-mail: loucibo@nbu.edu.cn
‡Corresponding author. E-mail: liangyi@gxu.edu.cn

© 2020 Chinese Physical Society and IOP Publishing Ltd

$$\varphi_m(x,y,z) = \mathrm{Ai}(s_{1m})\,\mathrm{Ai}(s_{2m})\exp(as_{1m}+as_{2m}),$$
$$s_{nm} = (-1)^n\cos(\theta/2)\,x/r_0 - \sin(\theta/2)\,y/r_0 + c_0,$$
$$\theta = (-1)^{m-1}\theta_0 + (-1)^{n-1}(m-1)\,2\pi/3,$$
$$n = 1,2, \quad m = 1,2,3, \tag{1}$$

where Ai(·) represents the Airy function, θ is the angle between two wings of each superposed 2D Airy beam, r_0 denotes an arbitrary transverse scale, s_n expresses a dimensionless transverse coordinate and a is an exponential decay factor, c_0 refers to the initial position of superposed 2D Airy beam, λ is the wavelength, and $k = 2\pi n/\lambda$ (n is the refractive index) is the wave number. Specifically, $a = 0.04$, $r_0 = 20$ μm, $c_0 = 1$, $\lambda = 632.8$ nm, $\theta = 75°$, $90°$, $110°$ are adopted in this work.

In experiment, we employed a setup similar to those in our previous work[29–31] to generate a three-Airy autofocusing beam (*i.e.*, via Fourier transforming a proper phase), as schematically shown in Fig. 1. The phase mask was obtained by summing three spectral phases associated with each 2D Airy beam, and was imposed on a spatial light modulator (SLM). Then, a linearly-polarized light ($\lambda = 632.8$ nm) illuminating on the SLM was modulated and further shaped into the AAF beams in the focal plane of a lens through a Fourier transformation. The propagation of the three-Airy autofocusing beam was monitored by scanning a CCD camera.

3. Results and discussion

Figures 1(b)–1(d) show side views of propagation for three-Airy autofocusing beams with $\theta = 75°$, $90°$, and $110°$, respectively. Figures 2(a)–2(c) show snapshots of the corresponding beam patterns of these beams at different propagation positions. At the input, the three 2D Airy beams are separated and have a distribution of threefold symmetry (see Figs. 2(a1)–2(c1)]. During propagation, they accelerate towards the center (see Figs. 2(a2)–2(c2)) and meet together at a certain propagation position (see Figs. 2(a3)–2(c3)), leading to a sharply focusing point and a large intensity enhancement. After the focusing point, they still propagate individually and do not affect their self-accelerating and non-diffracting propagation. Generally, after a longer propagation from the focal point, the whole three-Airy autofocusing beam starts to decrease in peak intensity, and its central main lobe gradually splits into three weaker subsequent main lobes (see Figs. 2(a4)–2(c4)). Then, an inverted triangular profile forms (see Figs. 2(a5)–2(c5)). As a result of the interference of three superposed 2D Airy beams, some new sidelobes appear among the subsequent main lobes. In the end, the three-Airy autofocusing beam shows a hexagonal shield shape (see Fig. 2(a6)–2(c6)).

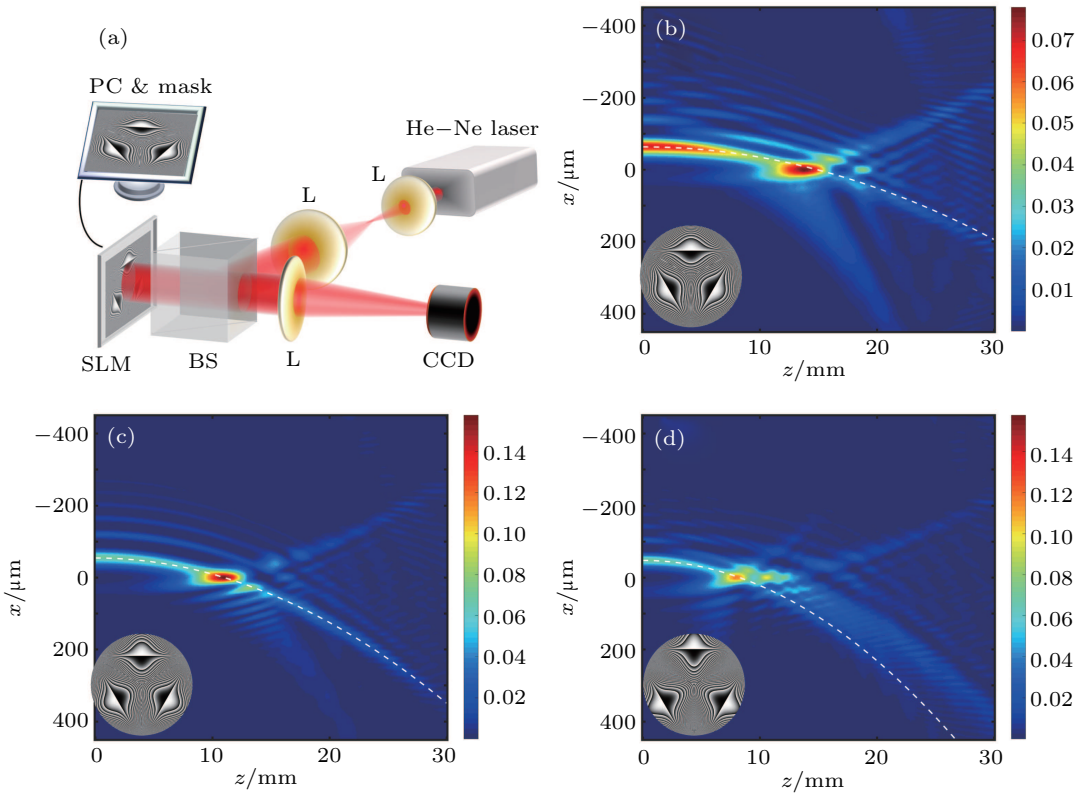


Fig. 1. (a) Schematic diagram of experimental setup, with L denoting lens, BS: beam splitter; SLM: spatial light modulator; sideview of 30-mm propagations of three-Airy autofocusing beams with different angles θ between two wings of each superposed 2D Airy beam: (b) 75°, (c) 90°, and (d) 110°. Insets in panels (b)–(d) show phase masks corresponding to $\theta = 75°$, $90°$, $110°$. The white dashed curves trace out Eq. (2), indicating trajectories of upper main lobes of three Airy autofocusing beams.

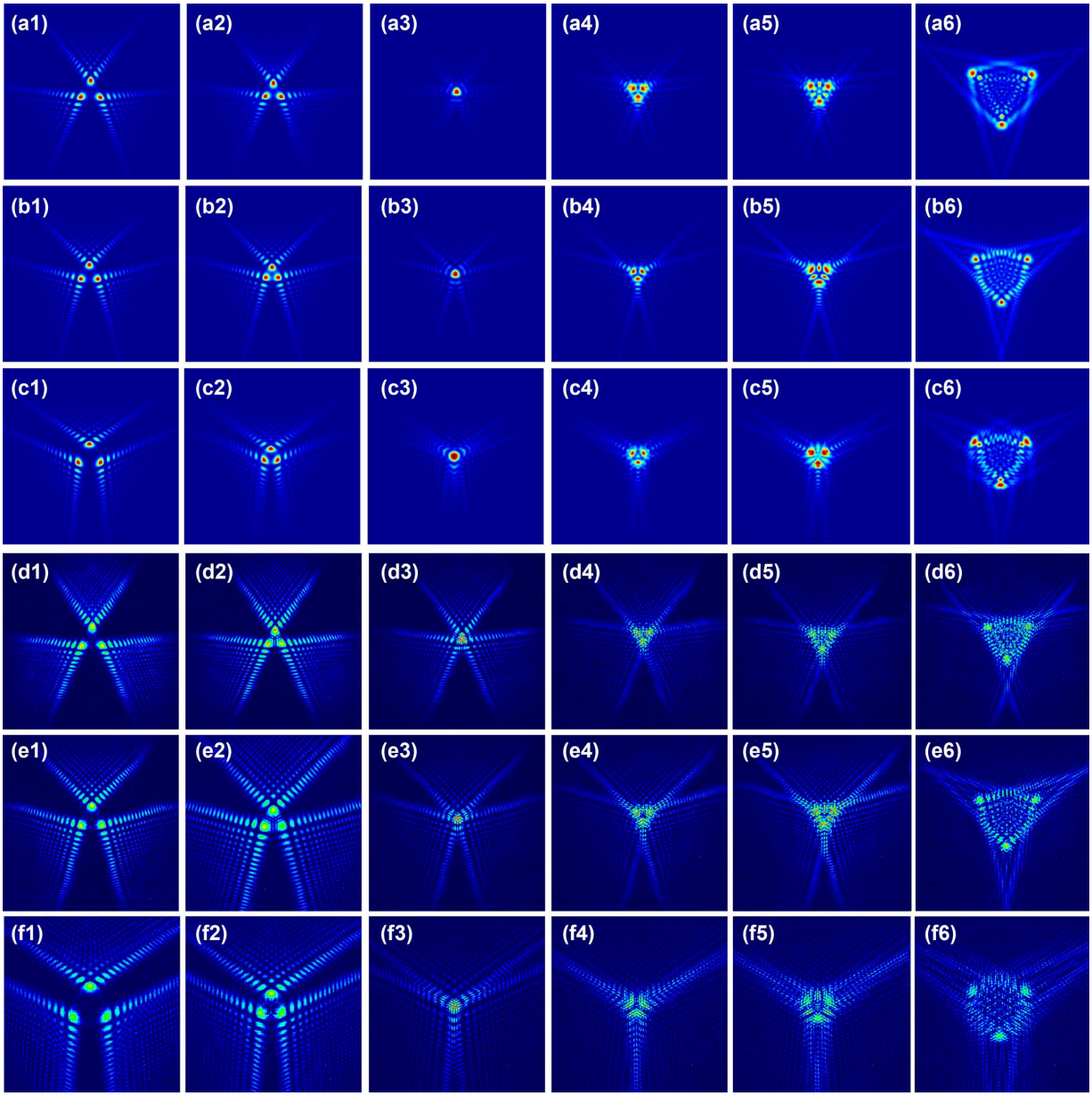


Fig. 2. Simulation results of beam transverse intensity patterns of three-Airy autofocusing beam with different initial wing angles: (a) $\theta = 75°$, (b) $\theta = 90°$, (c) $\theta = 110°$ at different propagation positions: [(a1)–(a6)] $z = 0$, 5, 14, 16, 19, 25 mm; [(b1)–(b6)] $z = 0$, 4, 11, 13, 15, 20 mm; [(c1)–(c6)] $z = 0$, 3, 8, 10, 12, 16 mm; [(d)–(f)] experimental results corresponding to panels (a)–(c).

In contrast, for the cases of $\theta \neq 90°$, the superposed three 2D Airy beams cannot maintain their shapes, particularly for a long distance propagation, because of a "hyperbolic umbilic" catastrophe as mentioned in Ref. [29]. Instead, their profiles tend to evolve into the 1D or 2D standard Airy patterns (see Figs. 2(a6) and 2(c6)). Moreover, the "hyperbolic umbilic" catastrophe divides the main lobe of the superposed three 2D Airy beams into two parts during propagation, leading to a less intense main lobe (see Figs. 1(b)–1(d)). Consequently, the peak intensity of the three-Airy autofocusing beam with $\theta \neq 90°$ at the focal point is weaker than that with $\theta = 90°$. For a detailed comparison, the intensity contrast $I_{\max}/I_0$ of three-Airy autofocusing beam versus angle θ is plotted in Fig. 3(a), where $I_{\max}$ and I_0 are the peak intensities at the focal point and the input, respectively. As expected, the three-Airy autofocusing beam reaches the maximum intensity contrast at $\theta = 90°$. The cases with $\theta < 90°$ have a larger negative influence on the intensity contrast than the case with $\theta > 90°$.

Also, from Fig. 1, it can be seen that the focusing length of three-Airy autofocusing beam varies with wing angle. Figure 3(b) presents their detailed relationship (black circle). The focusing length becomes shorter when wing angle θ is large. This can be understood by the fact that the acceleration a_θ of the superposed Airy beam increases as the value of θ rises up,[30] specifically, $a_\theta = \lambda^2 \sin^3(\theta/2)/4\pi^2 r_0^3$.

In theory, the initial position of the upper superposed Airy beam (see Figs. 2(a1)–2(c1)) is extracted by $y_{d0} = (-1.018 - c_0) r_0 / \sin(\theta/2)$ (Ai(-1.018) is the first local maximum of Ai(x)). Then, the trajectory of the main lobe of the upper superposed Airy beam can be described by the

following formula:

$$y_d = (-1.018 - c_0) r_0 / \sin(\theta/2) + \lambda^2 z^2 \sin^3(\theta/2)/4\pi^2 r_0^3. \quad (2)$$

Equation (2) is plotted with a white dash line in Figs. 1(b)–1(d). Comparing with the simulation results shown, equation (2) indeed describes the trajectory of the main lobe of the upper superposed Airy beam.

So, let $y_d = 0$, *i.e.*, three superposed Airy beams meet together at the focal point, then we will have a relation to calculate the focusing length F_z of three Airy autofocusing beams as follows:

$$F_z = \frac{2\pi r_0^2 \sqrt{(1.018 + c_0)}}{\lambda \sin^2(\theta/2)}. \quad (3)$$

This result is also plotted by a red solid line, which is in a good agreement with the simulation result shown in Fig. 3(b). In other words, the focusing length indeed decreases with wing angle θ increasing.

Similarly, we also analyze the effects of initial displacement (c_0) of the 2D Airy beams on their propagation as shown in Figs. 3(c) and 3(d). Obviously, the intensity contrast decreases with c_0 increasing. The focusing length increases with c_0 increasing, consistent with Eq. (3).

Figures 2(d)–2(f) show the experimental results, which agree well with the simulation results and the previous analysis: three-Airy autofocusing beam with larger initial wing angle θ has a smaller focusing length and only the superposed three-Airy beam in the case of $\theta = 90^\circ$ can maintain their profiles, *i.e.*, it does not experience deformation. In the case $\theta = 90^\circ$, the three-Airy autofocusing beam has a clearest hexagon edge pattern.

Next, the propagation of three-Airy autofocusing beam embedded an optical vortex phase with different topological charges L is also studied in simulation and experiments. The left three columns in Figs. 4 and 5 show the simulation results associated with two topological charges (*i.e.*, $L = 2$, 7), respectively. Comparing with the case of no vortex (Fig. 2), the superposed three-Airy beam exhibits a rotation during propagation (see Figs. 4(a1)–4(c1) and 5(a1)–5(c1)) and cannot focus into a single spot (see Figs. 4(a2)–4(c2) and 5(a2)–5(c2)), as a result of central singularity and the orbital angular momentum caused by the vortex phase. Finally, the main lobes cannot stay on the corners of the inverted triangular pattern (see Figs. 4(a3)–4(c3) and 5(a3)–4(c3)).

It should be noted that the rotation of three-Airy autofocusing beam is enhanced for larger topological charge that brings about larger orbital angular momentum. Specially, the rotation angle is proportional to the topological charge as shown in Fig. 3(e). In addition, the three main lobes of three-Airy autofocusing beam have somehow lateral shifting and cannot completely overlap each other at the focal point, causing a dark core in the center (see Figs. 4(a2)–4(c2)) and 5(a2)–5(c2)). Moreover, if the initial wing angle is larger, the dark core is smaller, indicating that the influence of topological charge decreases with a more opening initial wing angle θ. Actually, from Fig. 3(e), one can find that the rotation of the beam with bigger initial wing angle θ is smaller. In other words, a larger initial wing angle θ can suppress the rotation effect caused by the optical vortex. The right three columns in Figs. 4 and 5 show the experimental results. All of these results are in excellent agreement with the simulations.

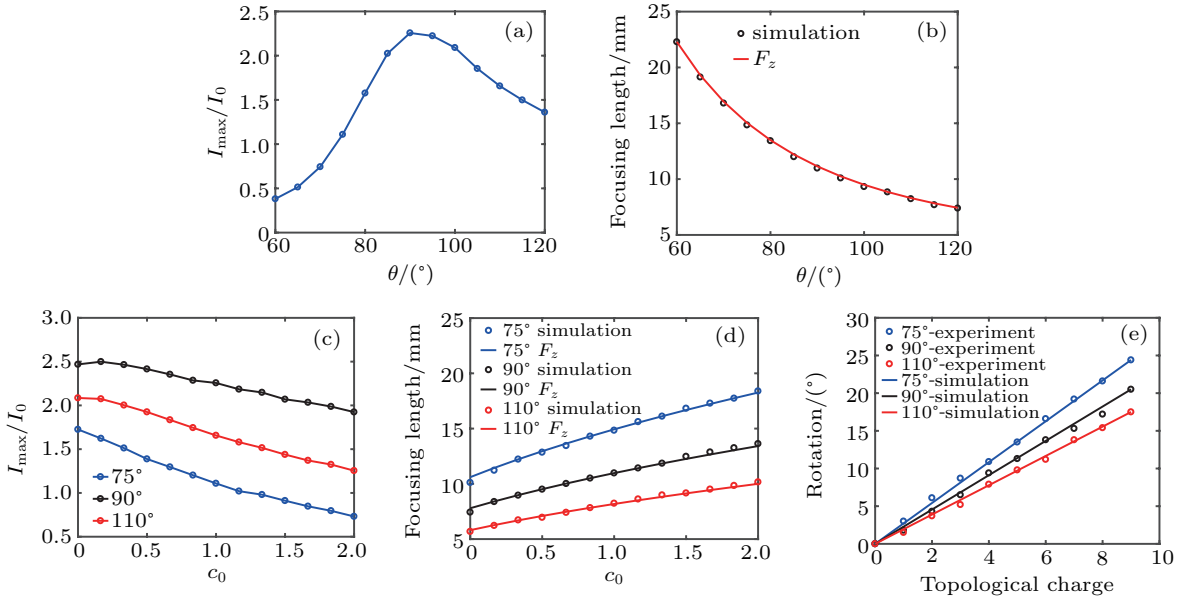


Fig. 3. (a) Intensity contrast I_{max}/I_0, (b) focusing length of three-Airy autofocusing beam with different initial wing angles, (c) intensity contrast I_{max}/I_0, (d) focusing length of three-Airy autofocusing beam with different values of initial c_0, with circles in panels (b)–(d) denoting simulation results and curve being calculated from Eq. (3), (e) rotation angles of three-Airy autofocusing beam carrying vortex as a function of topological charge for initial wing angle $\theta = 75^\circ$, 90°, 110°, respectively.

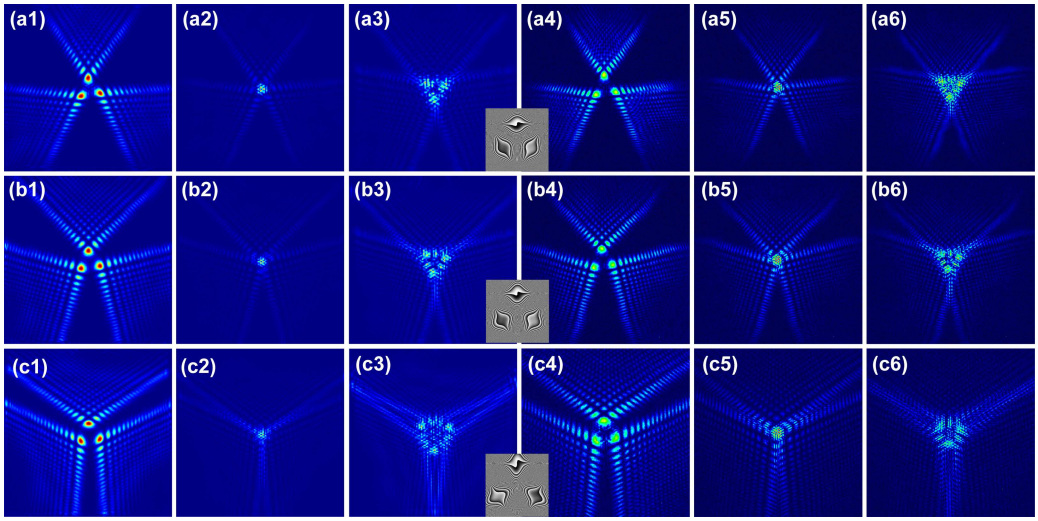


Fig. 4. Simulation results of the beam transverse intensity patterns of three-Airy autofocusing beam carrying $L = 2$ vortex with initial wing angle: $\theta = 75^\circ$ (a), 90° (b), and 110° (c) at propagation positions: $z = 3$ mm (a1), 14 mm (a2), 19 mm (a3), 2 mm (b1), 11 mm (b2), 15 mm (b3), 1 mm (c1), 8 mm (c2), and 13 mm (c3); Right three columns and central insets are for corresponding experimental results and phase mask, respectively.

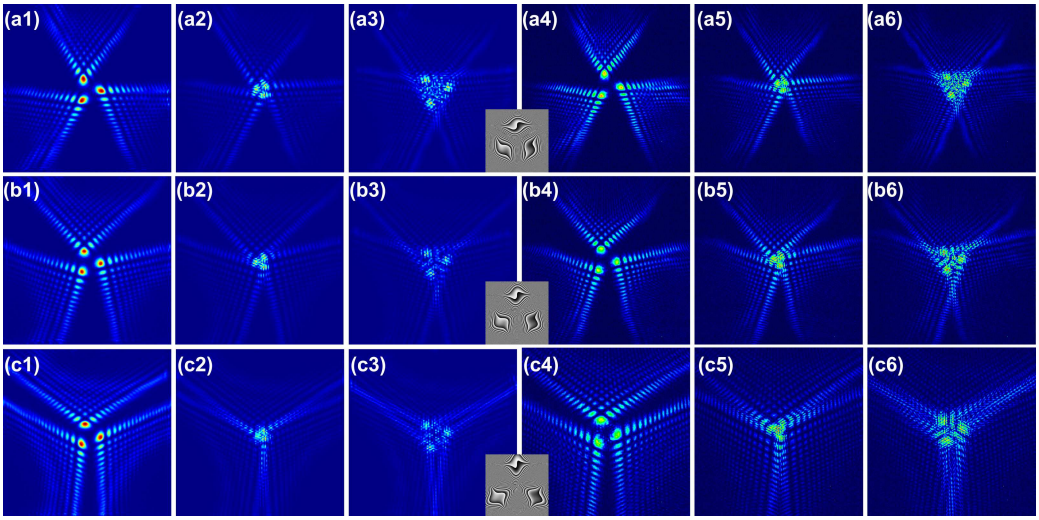


Fig. 5. Simulations of beam transverse intensity patterns of three-Airy autofocusing beam carrying $L = 7$ vortex with initial wing angle $\theta = 75^\circ$ (a), 90° (b), and 110° (c) at propagation positions $z = 3$ mm (a1), 14 mm (a2), 19 mm (a3), 2 mm (b1), 11 mm (b2), 15 mm (b3), 1 mm (c1), 8 mm (c2), and 12 mm (c3). Right three columns and central insets are for corresponding experimental results and phase mask.

4. Summary

In this work, we investigate the propagations of three-Airy autofocusing beam with different initial wing angles theoretically and experimentally. Our results show that the focusing length of the beam increases with initial wing angle turning small, due to the smaller transverse self-acceleration of the main lobes. However, the main lobes of three-Airy autofocusing beam with a non-90° wing angle shows a power separation in propagation, which is caused by "hyperbolic umbilic" catastrophe. Finally, the beam presents a strongest intensity contrast only in the case of 90°. Furthermore, when a vortex is imposed onto three-Airy autofocusing beams, a rotation proportional to topological charge appears. This rotation becomes weaker as the initial wing angle increases. Our result may be useful for designing and controlling the dynamical autofocusing beams for various applications such as optical manipulation.

References

[1] Siviloglou G A, Broky J, Dogariu A and Christodoulides D N 2007 *Phys. Rev. Lett.* **99** 213901
[2] Bandres M A, Kaminer I, Mills M, Rodríguez-Lara B M, Greenfield E, Segev M and Christodoulides D N 2013 *Opt. & Photon. News* **24** 30
[3] Efremidis N K, Chen Z G, Segev M and Christodoulides D N 2019 *Optica* **6** 686
[4] Baumgartl J, Mazilu M and Dholakia K 2008 *Nat. Photon.* **2** 675
[5] Zhang P, Prakash J, Zhang Z, Mills M S, Efremidis N K, Christodoulides D N and Chen Z G 2011 *Opt. Lett.* **36** 2883
[6] Polynkin P, Kolesik M, Moloney J V, Siviloglou G A and Christodoulides D N 2009 *Science* **324** 229
[7] Chong A, Renninger W H, Christodoulides D N and Wise F W 2010 *Nat. Photon.* **4** 103
[8] Rose P, Diebel F, Boguslawski M and Denz C 2013 *Appl. Phys. Lett.* **102** 101101
[9] Jia S, Vaughan J C and Zhuang X W 2014 *Nat. Photon.* **8** 302

[10] Vettenburg T, Dalgarno H I C, Nylk J, Coll-Lladó C, Ferrier D E K, Čižmár T, Gunn-Moore F J and Dholakia K 2014 *Nat. Methods* **11** 541
[11] Liang Y, Hu Y, Song D H, Lou C B, Zhang X Z, Chen Z G and Xu J J 2015 *Opt. Lett.* **40** 5686
[12] Kondakci H E and Abouraddy A F 2017 *Nat. Photon.* **11** 733
[13] Nylk J, McCluskey K, Preciado M A, Mazilu M, Yang Z Y, Gunn-Moore F J, Aggarwal S, Tello J A, Ferrier D E K and Dholakia K 2018 *Sci. Adv.* **4** eaar4817
[14] Clerici M, Hu Y, Lassonde P, Milián C, Couairon A, Christodoulides D N, Chen Z G, Razzari L, Vidal F, Légaré F, Faccio D and Morandotti R 2015 *Sci. Adv.* **1** e1400111
[15] Mathis A, Courvoisier F, Froehly L, Furfaro L, Jacquot M, Lacourt P A and Dudley J M 2012 *Appl. Phys. Lett.* **101** 071110
[16] Salandrino A and Christodoulides D N 2010 *Opt. Lett.* **35** 2082
[17] Zhang P, Wang S, Liu Y M, Yin X B, Lu C G, Chen Z G and Zhang X 2011 *Opt. Lett.* **36** 3191
[18] Minovich A, Klein A E, Janunts N, Pertsch T, Neshev D N and Kivshar Y S 2011 *Phys. Rev. Lett.* **107** 116802
[19] Zhang P, Li T C, Zhu J, Zhu X F, Yang S, Wang Y, Yin X B and Zhang X 2014 *Nat. Commun.* **5** 4316
[20] Voloch-Bloch N, Lereah Y, Lilach Y, Gover A and Arie A 2013 *Nature* **494** 331
[21] Efremidis N K and Christodoulides D N 2010 *Opt. Lett.* **35** 4045
[22] Papazoglou D G, Efremidis N K, Christodoulides D N and Tzortzakis S 2011 *Opt. Lett.* **36** 1842
[23] Chen B, Chen C D, Peng X, Peng Y L, Zhou M L and Deng D M 2015 *Opt. Express* **23** 19288
[24] Chen X Y, Deng D M, Zhuang J L, Yang X B, Liu H Z and Wang G H 2018 *Appl. Opt.* **57** 8418
[25] Chen X Y, Zhuang J L, Peng X L, Li D D, Zhang L P, Zhao F and Deng D M 2019 *Opt. Laser Technol.* **109** 518
[26] Deng D M, Gao Y M, Zhao J Y, Zhang P and Chen Z G 2013 *Opt. Lett.* **38** 3934
[27] Chen X Y, Deng D M, Zhuang J L, Peng X, Li D D, Zhang L P, Zhao F, Yang X B, Liu H Z and Wang G H 2018 *Opt. Lett.* **43** 3626
[28] Zhang Z, Ye Z Y, Song D H, Zhang P and Chen Z 2013 *Appl. Opt.* **52** 8512
[29] Liang Y, Hu Y, Ye Z Y, Song D H, Lou C B, Zhang X Z, Xu J J, Morandotti R and Chen Z G 2014 *J. Opt. Soc. Am. A* **31** 1468
[30] Qian Y X and Dong L W 2015 *Appl. Opt.* **54** 10487
[31] Chen Y K, Lin X W, Lin S Y, Mo S Y, Wan L Y and Liang Y 2017 *Chin. Opt. Lett.* **15** 080801